arXiv:1612.02176v2 [cond-mat.mes-hall] 3 Mar 2017

Exotic surface states in hybrid structures of topological insulators and Weyl semimetals

Stefan Juergens and Björn Trauzettel
Institute of Theoretical Physics and Astrophysics, University of Würzburg, D-97074 Würzburg, Germany
(Dated: March 6, 2017)

Topological insulators (TIs) and Weyl semimetals (WSMs) are two realizations of topological matter usually appearing separately in nature. However, they are directly related to each other via a topological phase transition. In this paper, we investigate the question whether these two topological phases can exist together at the same time, with a combined, hybrid surface state at the joint boundaries. We analyze effective models of a 3D TI and an inversion symmetric WSM and couple them in a way that certain symmetries, like inversion, are preserved. A tunnel coupling approach enables us to obtain the hybrid surface state Hamiltonian analytically. This offers the possibility of a detailed study of its dispersion relation depending on the investigated couplings. For spin-symmetric coupling, we find that two Dirac nodes can emerge out of the combination of a single Dirac node and a Fermi arc. For spin-asymmetric coupling, the dispersion relation is gapped and the former Dirac node gets spin-polarized. We propose different experimental realization of the hybrid system, including compressively strained HgTe as well as heterostructures of TI and WSM materials.

PACS numbers:

I. INTRODUCTION

The study of topological properties in a semiconductor environment has become a strong and flourishing field in condensed matter physics. Topological insulators (TIs) are the standard materials in this context, well studied both theoretically and experimentally by now[1–3]. Their semi-metallic counter-parts, Weyl semimetals (WSMs)[4–7], were also proposed to exist in condensed matter systems decades ago[8–10]. However, only very recently with the prediction of concrete material realizations[11–13] the field has seen an enormous growth. The experimental proof of the existence of Weyl points and their corresponding surface states, called Fermi arcs, followed soon afterwards[14–19]. Yet both for fundamental research and application purposes these "early" WSMs, such as the TaAs family of non-centrosymmetric monopnictides, are too complicated with many Weyl points (24 for TaAs) in the Brillouin zone. Simpler materials with eight[20–29] and four[30,31] Weyl points have been predicted and observed, where the latter is the minimal number of Weyl points for a system with time-reversal symmetry (TRS). Materials with broken TRS[32] could realize the absolute minimum of two Weyl points, but for that case only theoretical proposals[33–37] exist so far. Most of them rely on magnetically doped TIs or TI heterostructures.

TI and WSM are both topological phases that can be directly connected to each other through quantum phase transitions[10,38]. In this paper we want to go a step further and study the question whether a system can be both in the TI and WSM phase at the same time, or at least support both corresponding surface states, 2D Dirac surface states and Fermi arcs, on the same surface.

Such a combined phase might exist in HgTe with applied compressive strain. The strain pushes the Γ_8 bands into one another, creating Dirac points which are then split by breaking of inversion symmetry through bulk inversion asymmetry (BIA) terms[26]. At the same time, the topological band inversion between the Γ_8 and the Γ_6 bands remains, leading to the conjecture that this system could have topological Dirac states and Fermi arcs on its surface.

A different way to create such a hybrid surface state is placing a TI and WSM spatially adjacent to each other, possibly separated by a small, topological trivial buffer layer. The separate surface states of TI and WSM will interact, e.g. by Coulomb interaction or tunneling due to a small overlap of wave functions, forming the hybrid surface dispersion relation. Previous related research on adjacent TI and WSM phases[39] suggest that at such a shared surface both Dirac states and Fermi arcs can exist. However, they were found in different areas of k-space, mutually excluding one another such that they do not hybridize at all. Our approach differs from the one chosen in Ref. 39 by considering only a small, perturbative coupling between the two phases. This ensures that both TI and WSM surface states survive and can interact with each other.

We focus in this paper on an analytical study of the combined surface states generated from the hybridized TI and WSM. A simplified ansatz offers the possibility to calculate the surface Hamiltonian analytically, allowing for a detailed analysis of the surface physics. Depending on the symmetry of the assumed couplings, the surface dispersion relation shows quite different behavior. In the case of spin symmetry, two shifted Dirac nodes may emerge out of the combination of a single Dirac node and a Fermi arc. For spin-asymmetric coupling, the Fermi arc gaps out and spin-polarizes the former Dirac node.

The article is organized as follows. We recap effective

models for the separate phases of TIs and WSMs[38,40–43] and discuss their symmetry properties and surface states in Sec. II. The coupling of the Hamiltonians and the analytic form of the surface state is discussed in Sec. III. Sec. IV focuses on the different ways to influence and tune the combined surface dispersion relation. Possible experimental realizations are proposed in Sec. V.

II. SEPARATE MODELS

The model of the TI phase we will use was originally derived for the Bi_2Se_3 family of materials in Refs. 40, 41. It contains four bands and serves as a minimal, but general, TI model. The Weyl Hamiltonian considered in the following originates from Refs. 42,43. It contains two bands and models an inversion symmetric type I or II WSM with two Weyl points. We simplify the models as far as possible without losing too much versatility. It is important to retain terms quadratic in momentum for the introduction of the surface in the z direction. This is done via hardwall boundary conditions on a half space $z \leq 0$ or $z \geq 0$.

A. Topological Insulator

The effective Hamiltonian for a 3D TI is given by the 4x4 matrix[40,41]

$$H_{TI} = \begin{pmatrix} M(k)\tau_3 + Bk_z\tau_2 + C\tau_0 & iAk_-\tau_1 \\ -iA^*k_+\tau_1 & M(k)\tau_3 + Bk_z\tau_2 + C\tau_0 \end{pmatrix} \tag{2.1}$$

with $M(k) = M_0 + M_1\left(k_\parallel^2 + k_z^2\right)$, $k_\parallel^2 = k_x^2 + k_y^2$ and $k_\pm = k_x \pm ik_y = k_\parallel e^{\pm i\phi_k}$. In the original derivation for Bi_2Se_3 the Pauli matrices $\vec{\tau}$ describe an orbital degree of freedom. H_{TI} is written in a spin-up/down basis, represented by the Pauli matrices $\vec{\sigma}$ in the following. The coupling $A = |A|\, e^{i\phi_A}$ can in principle be complex. The model is in the strong TI phase for $M_0 M_1 < 0$.

We define the inversion operator $P_{TI} = \sigma_0 \otimes \tau_3$ and time-reversal operator $T_{TI} = i\sigma_2 \otimes \tau_0 K$ with K the complex conjugation operator. H_{TI} is symmetric under both operations, fulfilling

$$\begin{aligned} P_{TI}^\dagger H_{TI}(-k) P_{TI} &= H_{TI}(k), \\ T_{TI}^\dagger H_{TI}(-k) T_{TI} &= H_{TI}(k). \end{aligned} \tag{2.2}$$

The bulk dispersion relation is double degenerate and given by

$$E_{TI} = C \pm \sqrt{|A|^2 k_\parallel^2 + B^2 k_z^2 + M(k)^2}. \tag{2.3}$$

Based on the method described in App. A, the surface states can be calculated analytically. We assume opposite surfaces to be well separated, which offers the possibility to treat them individually. Thus in the calculation we only consider one of them via hardwall boundary conditions at $z = 0$. The surface wave function is then given by

$$\Psi(z) = \frac{1}{\sqrt{2}}\left(e^{ik_{z,1}z} - e^{ik_{z,2}z}\right)\begin{pmatrix} \pm\frac{i\eta Ak_-}{|A|k_\parallel}\psi_\eta \\ \psi_\eta \end{pmatrix} \tag{2.4}$$

with $\psi_\eta = \frac{1}{\sqrt{2}}\begin{pmatrix} 1 \\ \eta \end{pmatrix}$ and the inverse localization length $ik_{z,\frac{1}{2}} = \frac{1}{2M_1}\left[-\eta B \pm \sqrt{4M_1\left(M_0 + M_1 k_\parallel^2\right) + B^2}\right]$. The sign $\eta = \pm$ depends on the surface, $\eta = -\mathrm{sgn}\left(\frac{B}{M_1}\right)$ (upper surface) or $\eta = \mathrm{sgn}\left(\frac{B}{M_1}\right)$ (lower surface).

The existence condition for the surface state, see App. A, is

$$M_1\left(M_0 + M_1 k_\parallel^2\right) < 0 \tag{2.5}$$

stressing the importance of being in the inverted regime.

The surface Hamiltonian (dispersion relation) is obtained from H_{TI} by projecting out the orbital (orbital & spin) degrees of freedom with the help of ψ_η ($\Psi(z)$). We find the usual Dirac form

$$H_{TI}^{sur} = \begin{pmatrix} C & i\eta Ak_- \\ -i\eta A^*k_+ & C \end{pmatrix};\ E_{TI}^{sur} = C \pm |A|\, k_\parallel, \tag{2.6}$$

experiencing spin-momentum locking, with the angle $\phi_A + \frac{\eta\pi}{2}$ between the spin projection and momentum vector in the x-y plane. The combined dispersion relations of the bulk and surface of the TI are shown in Fig. 1.

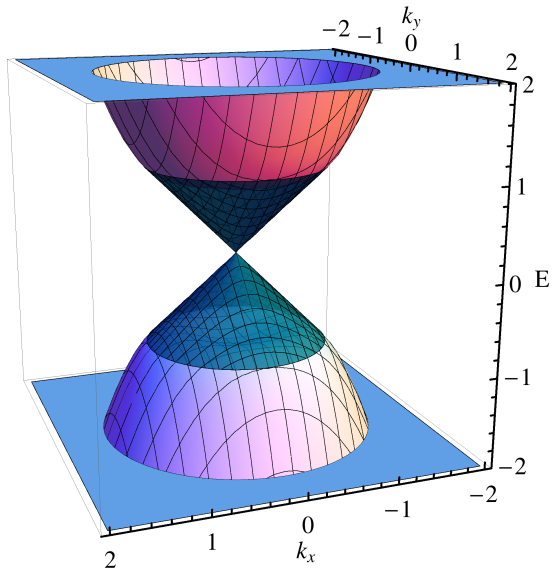

FIG. 1: Bulk and surface dispersion relations, Eqs. (2.3) and (2.6), of the TI model. The surface band is plotted in cyan. Parameters: $C = 0$, $M_0 = -1$, $M_1 = 1$, $A = 1$, $B = 1$, $k_z = 0$.

B. Inversion symmetric Weyl Semimetal

A WSM exists in different flavors. On the one hand, one distinguishes type I and type II depending on preserved or broken Lorentz invariance at the Weyl points[44–46]. Secondly, either time-reversal or inversion symmetry has to be broken to get from a Dirac to a Weyl semimetal. For all these phases minimal models have been proposed in the literature[38,42,43,47].

For simplicity, we focus on the model with broken time-reversal and preserved inversion symmetry, as it has the minimal number of one pair of Weyl points. The Hamiltonian is

$$H_W = t(k)\tau_3 + v_z k_z \tau_2 + v_y k_y \tau_1 + \gamma t\left(k_x^2 - k_W^2\right)\tau_0 \quad (2.7)$$

with $t(k) = t\left(k_\parallel^2 + k_z^2 - k_W^2\right)$. The degree of freedom described by the Pauli matrices $\vec{\tau}$ can be orbital, spin or a combination of the two, depending on the specific material realization. For the concrete form of the symmetry operations considered in the following we assume a spinless system[43]. The two Weyl points are specified by $k_x = \pm k_W$. The parameter γ leads to a tilting of the dispersion relation at the Weyl points. For $|\gamma| < 1$ one has a type I, otherwise a type II WSM. Expanding H_W around $k_x = \pm k_W$ yields a Hamiltonian with linearized Weyl form

$$H_W^{lin} = v_y k_y \tau_1 + v_z k_z \tau_2 \pm 2t k_W k_x \left(\tau_3 + \gamma\tau_0\right). \quad (2.8)$$

The Hamiltonian H_W fulfills the symmetry conditions

$$\begin{aligned} P_W^\dagger H_W(-k) P_W &= H_W(k), \\ T_W^\dagger H_W(-k) T_W &\neq H_W(k) \end{aligned} \quad (2.9)$$

with the inversion operator $P_W = \tau_3$ and time-reversal operator $T_W = \tau_0 K$ with K the complex conjugation operator. Hence, parity is preserved and time-reversal symmetry broken.

The bulk dispersion relation is then given by

$$E_W = \gamma t\left(k_x^2 - k_W^2\right) \pm \sqrt{v_y^2 k_y^2 + v_z^2 k_z^2 + t(k)^2}. \quad (2.10)$$

The surface states can be calculated analytically based on the method discussed in the App. A. Their wave function is given by

$$\Psi(z) = \left(e^{ik_{z,1}z} - e^{ik_{z,2}z}\right)\psi_\eta \quad (2.11)$$

with $\psi_\eta = \frac{1}{\sqrt{2}}\begin{pmatrix} 1 \\ \eta \end{pmatrix}$ and inverse localization length $ik_{z,\frac{1}{2}} = \frac{1}{2t}\left[-\eta v_z \pm \sqrt{4t^2\left(k_\parallel^2 - k_W^2\right) + v_z^2}\right]$. The sign $\eta = \pm$ depends on the surface; $\eta = -\mathrm{sgn}\left(\frac{v_z}{t}\right)$ (upper surface) or $\eta = \mathrm{sgn}\left(\frac{v_z}{t}\right)$ (lower surface).

The existence condition for the surface state is

$$k_\parallel^2 < k_W^2 \quad (2.12)$$

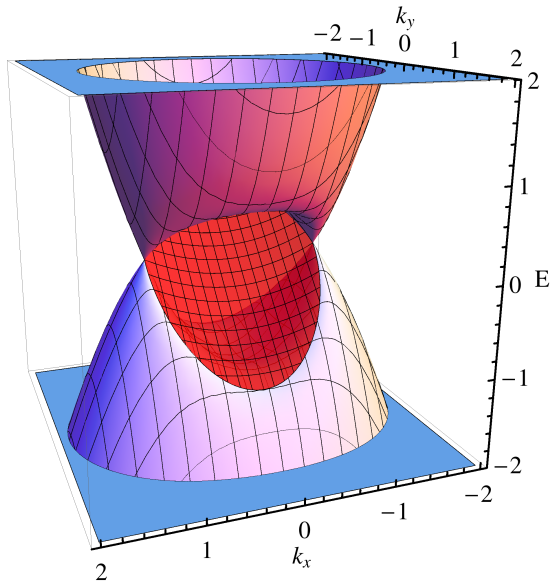

FIG. 2: Bulk and upper surface dispersion relations, Eqs. (2.10) and (2.13), of the Weyl model. The surface band is plotted in red.
Parameters: $\gamma = \frac{1}{4}$, $k_W = 1$, $t = 1$, $v_y = 1$, $v_z = 1$, $k_z = 0$.

such that Fermi arcs can only exist between the Weyl points.

Hence, the surface dispersion relation yields the known Fermi arc spectrum

$$E_W^{sur} = \gamma t\left(k_x^2 - k_W^2\right) + \eta v_y k_y. \quad (2.13)$$

The combined dispersion relations of the bulk and surface of the WSM are shown in Fig. 2.

III. COUPLED SYSTEM

The Hamiltonians and surface wave functions of the TI and WSM phases discussed in Sec. II are very similar. Thus, we conjecture that also the combined system may have surface states which can be calculated by the simplified method described in App. A. This will allow us to discuss the surface physics analytically.

In this section, we define the combined Hamiltonian and discuss the couplings allowed by symmetry under the assumptions that certain symmetries are preserved. The surface state Hamiltonian and wave function are derived and the limitations due to the approximated calculation method are discussed.

The combined Hamiltonian of the TI and WSM phases is defined by

$$H_{WTI} = \begin{pmatrix} H_{TI} & H_C \\ H_C^\dagger & H_W \end{pmatrix} \quad (3.1)$$

with the coupling H_C. Such a coupling can be regarded as a tunneling Hamiltonian approach where H_C (weakly)

couples the two entities H_{TI} and H_W. A similar approach has been considered in Ref. 48 to combine topological systems of different kinds with each other and study their emerging physics. The combined symmetry operator for inversion symmetry is now given by

$$P_{WTI} = \begin{pmatrix} P_{TI} & 0 \\ 0 & P_W \end{pmatrix}. \tag{3.2}$$

As time-reversal symmetry is already broken in the subsystem of the WSM, it will also be absent in the combined system. The study of the effect on the TI of such a breaking of time-reversal symmetry via coupling, applicable e.g. in the setup of spatially separate Weyl and TI phases as depicted in Fig. 8 (b), is one of the goals of this paper. The stability of gapless edge states to time-reversal symmetry breaking perturbations such as magnetic fields[49] and considerable Coulomb interaction[50] is an active research topic and has been experimentally observed in 2D. It is proposed that crystalline symmetries such as inversion or rotational symmetries protect the gapless edge states in the absence of time-reversal symmetry. As inversion symmetry is preserved in our system, we conjecture that the use of the gapless TI model can be justified even in a time-reversal breaking environment.

Applying the inversion operator to the Hamiltonian, following Eqs. (2.2) and (2.9), yields restrictions for the allowed couplings assuming that this symmetry is not broken. As the symmetry operator is block-diagonal, these restrictions do not depend on H_W or H_{TI}.

For an inversion symmetric system, the couplings proportional to τ_3 and τ_0 have to be even in momentum, while the ones proportional to τ_2 and τ_1 have to be odd in momentum. We choose the following representation

$$H_{C,IS} = \begin{pmatrix} H_{c,IS} \\ \tilde{H}_{c,IS} \end{pmatrix} \tag{3.3}$$

with

$$H_{c,IS} = d(k_\parallel)\tau_3 + c_1 k_+ \tau_2 + b_1 k_+ \tau_1 + a(k_\parallel)\tau_0, \tag{3.4}$$

where $d(k_\parallel) = d_0 + d_2 k_\parallel^2$, $a(k_\parallel) = a_0 + a_2 k_\parallel^2$, and $\tilde{H}_{c,IS}$ having the same structure. This choice ensures the preservation of parity for the combined system. The size of the terms depends on the concrete experimental realization, where the best candidate materials for our proposal have yet to be identified. In the case of two spatially separate Weyl and TI systems, as depicted in Fig. 8 (b), the coupling parameters can be calculated from the overlap of the wave functions of the different materials. As an example, this is done in Ref. 51 for a bilayer HgTe quantum well system by fitting a $\mathbf{k}\cdot\mathbf{p}$ model to experimentally obtained band structures. In general, all symmetry allowed couplings can be relevant for the following discussion.

In this paper however, coupling terms proportional to k_z are not considered, for simplicity. This is a physically reasonable assumption at least for the surface states if one assumes them to be 2D, perfectly localized in the z-direction. Close to the Weyl points or the TI bulk band edge where the surface states delocalize a k_z dependent coupling should be taken into account.

The ansatz we will consider is

$$\Psi(z) = \left(e^{ik_{z,1}z} - e^{ik_{z,2}z}\right) \begin{pmatrix} L_1(k_\pm)\,\psi_{\eta_{TI}} \\ L_2(k_\pm)\,\psi_{\eta_{TI}} \\ L_3(k_\pm)\,\psi_{\eta_W} \end{pmatrix} \tag{3.5}$$

with $\psi_\eta = \frac{1}{\sqrt{2}}\begin{pmatrix} 1 \\ \eta \end{pmatrix}$. This is a special case of the general form of the surface wave function $\Psi_g(z) = \sum_j a_j e^{ik_{z,j}z}\psi(k_\pm, k_{z,j})$, $j \in \{1, ..., 6\}$. Its choice is motivated by the ability to obtain analytical solutions for the surface states. Physically it means that we only consider solutions were the TI and WSM surface states have the same exponential localization with the same localization length. This implies that phase transitions of the subsystems, such as normal insulator (NI) to TI or NI to WSM, can not be discussed separatly in this treatment. However, for a system deep in the TI and WSM phase, the simplification should not alter the essential physics. We have checked numerically that small differences in the localization lengths of the subsystems do not alter the surface dispersion relations in a qualitative way, see App. B.

Projecting the Hamiltonian Eq. (3.1) on the surface, this separates the eigenvalue equation into simpler problems

$$H^{sur}_{WTI}\begin{pmatrix} L1 \\ L2 \\ L3 \end{pmatrix} = E^{sur}_{WTI}\begin{pmatrix} L1 \\ L2 \\ L3 \end{pmatrix}, \tag{3.6}$$

$$H^{k_z}_{WTI}\begin{pmatrix} L1 \\ L2 \\ L3 \end{pmatrix} = 0 \tag{3.7}$$

with the Hamiltonians

$$H^{sur}_{WTI} = \begin{pmatrix} C & i\eta A k_- & a(k_\parallel)+\eta b_1 k_+ \\ -i\eta A^* k_+ & C & \tilde{a}(k_\parallel)+\eta\tilde{b}_1 k_+ \\ a(k_\parallel)^*+\eta b_1^* k_- & \tilde{a}(k_\parallel)^*+\eta\tilde{b}_1^* k_- & \gamma t\left(k_x^2-k_W^2\right)+\eta v_y k_y \end{pmatrix}, \tag{3.8}$$

$$\underset{part.\ diag.}{\Rightarrow} \begin{pmatrix} C+|A|\,k_\parallel & 0 & \tilde{H}_c+e^{i\phi_k^A}H_c \\ 0 & C-|A|\,k_\parallel & \tilde{H}_c-e^{i\phi_k^A}H_c \\ \tilde{H}_c^*+e^{-i\phi_k^A}H_c^* & \tilde{H}_c^*-e^{-i\phi_k^A}H_c^* & \gamma t\left(k_x^2-k_W^2\right)+\eta v_y k_y \end{pmatrix}, \tag{3.9}$$

$$H^{k_z}_{WTI} = \begin{pmatrix} M(k)-i\eta B k_z & 0 & d(k_\parallel)-i\eta c_1 k_+ \\ 0 & M(k)-i\eta B k_z & \tilde{d}(k_\parallel)-i\eta\tilde{c}_1 k_+ \\ d(k_\parallel)^*-i\eta c_1^* k_- & \tilde{d}(k_\parallel)^*-i\eta\tilde{c}_1^* k_- & t(k)-i\eta v_z k_z \end{pmatrix} \tag{3.10}$$

for $\eta = \eta_{TI} = \eta_W$. In Eq. (3.9), we partially diagonalize the Hamiltonian and define $\phi_k^A = \phi_k - \phi_A - \eta\frac{\pi}{2}$, $H_c = a(k_\parallel)+\eta b_1 k_+$ and $\tilde{H}_c = \tilde{a}(k_\parallel)+\eta\tilde{b}_1 k_+$. This will help in the interpretation of the surface dispersion relation in terms of coupled Dirac cone and Fermi arc. In the case of $\eta = \eta_{TI} = -\eta_W$, one has to replace in Eqs. (3.8) - (3.10) $a(k_\parallel) \leftrightarrow d(k_\parallel)$, $b_1 \leftrightarrow ic_1$, $v_y \to -v_y$ and $v_z \to -v_z$. We will focus in the following on the former, $\eta_{TI} = \eta_W$, case. Taking $\begin{pmatrix} L1 & L2 & L3 \end{pmatrix}^T$ as the same eigenvector in Eqs. (3.6) and (3.7), the latter can only be fulfilled by further restrictions on the parameters. We choose a locking between some of the TI and the WSM parameters, i.e. $t(k) = \nu M(k)$ and $v_z = \nu B$ with ν a constant (set to 1 in the following). This ensures the same localization length for the two subsystems. Additionally, the couplings c_1 and $d(k_\parallel)$ are set to be 0 for simplicity. Therefore the total coupling does not change the original orbital character of the TI and WSM surface states, being eigenstates of the τ_1 matrix with fixed eigenvalue + or −. With regard to these restrictions, we have checked that the neglected couplings can be considered numerically with only quantitative changes to the surface dispersion relations, see App. B.

In total, this leads to the same quadratic equation for k_z as in the pure TI case, $ik_{z,\frac{1}{2}} = \frac{1}{2M_1}\left[-\eta B \pm \sqrt{4M_1\left(M_0+M_1 k_\parallel^2\right)+B^2}\right]$. The existence condition is again

$$M_1\left(M_0+M_1 k_\parallel^2\right) < 0 \tag{3.11}$$

and the (unnormalized) eigenvectors are given by

$$\begin{pmatrix} L1 \\ L2 \\ L3 \end{pmatrix} = \begin{pmatrix} \left(E^{sur}_{WTI}-C\right)H_c + i\eta A k_- \tilde{H}_c \\ \left(E^{sur}_{WTI}-C\right)\tilde{H}_c - i\eta A^* k_+ H_c \\ \left(E^{sur}_{WTI}-C\right)^2 - |A|^2 k_\parallel^2 \end{pmatrix}. \tag{3.12}$$

The eigenenergies E^{sur}_{WTI} are too lengthy to state them here, but can also be derived analytically.

The obtained solution leads to the possibility to tune bulk and surface dispersion relations rather independently. Parameters M_i and B influence the surface dispersion relation only indirectly via the existence condition and finite γ parameter, while they strongly influence the bulk band structure as will be shown in the next section. Tuning the coupling constants v_y, A, $a\left(k_\parallel\right)$, b_1 and their relative phase will still provide a rich parameter space to be explored below.

IV. SURFACE DISPERSION RELATION

In this section, we discuss the influence of the different coupling parameters on the combined surface states of TIs and WSMs. Depending on the choice of symmetries of the coupling, observed phenomenas are the generation of additional Dirac points in the dispersion relation or the spin polarization of certain surface bands.

A. Uncoupled scenario

Beginning with the uncoupled case, $H_{C,IS} = 0$, the dispersion relations of the surface and bulk states are shown in Fig. 3. The black lines denote the bulk dispersion relation, cyan (from blue (green) for spin up (down)) and red stand for the TI and WSM surface states, respectively. The two black dots give the position of the bulk Weyl points. We note that the surface states originate at the bulk states, but cross them unaffectedly. Together with the fact that one can tune the bulk gap M_0 without changing the surface dispersion relation (aside from the existence condition), we find the possibility to discuss the bulk and surface dispersion relations rather separately from each other. It will always be possible to increase the bulk gap and the distance between the two Weyl points such that the interesting surface physics happens in regions of the Brillouin zone where no bulk state is located. Therefore, we will focus in the following on tuning of the surface dispersion relation only. In numerical calculations, see App. B, purely exponentially decaying surface states do not coexist with bulk states at the same energy and momenta. This is due to finite hybridization between the bulk and surface states.

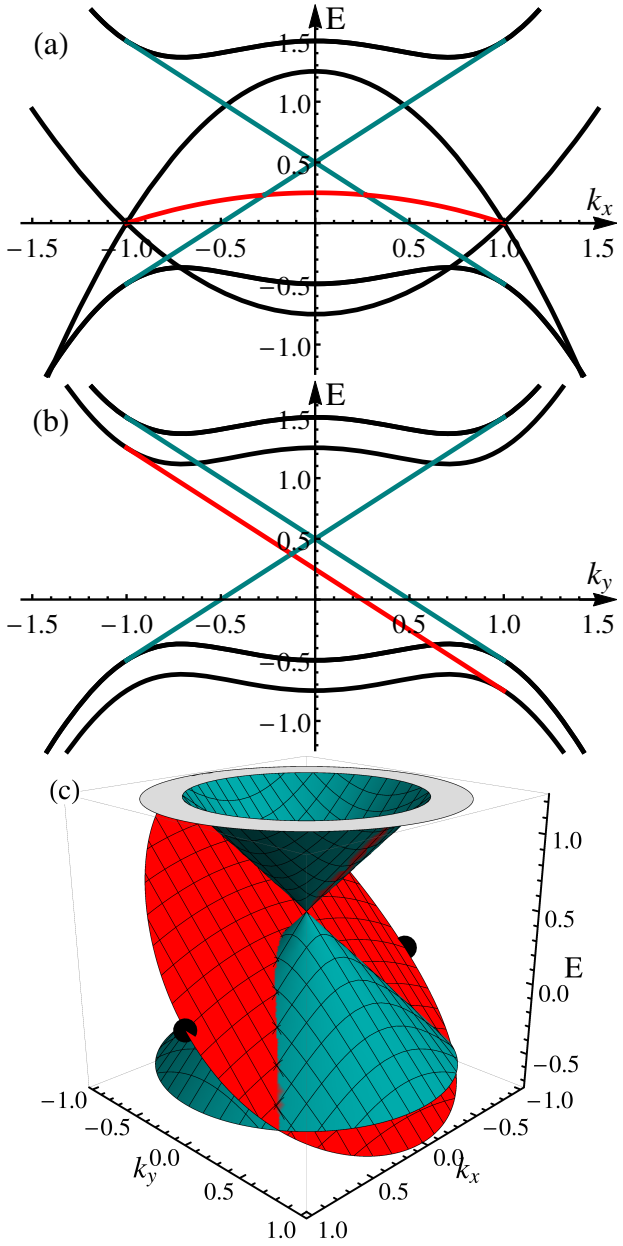

FIG. 3: (a) and (b) Bulk and upper surface dispersion relations of the uncoupled TI and WSM models. Color code: Black lines for the bulk states, red for WSM character and cyan for the TI character of the surface states. (c) 3D plot of the surface dispersion relation. The two black dots denote the position of the bulk Weyl points.
Parameters: $C = \frac{1}{2}$, $M_0 = -1$, $M_1 = 1$, $B = 1$, $k_z = 0$, $\gamma = -\frac{1}{4}$, $A = 1$, $v_y = 1$, $a(k_\parallel) = b_1 = 0$, $H_c = \tilde{H}_c$.

B. Real, spin-symmetric coupling: Creation of additional Dirac points

A straight-forward way to couple TI and WSM is a real and spin-symmetric coupling via $a(k_\parallel) > 0$ or $b_1 > 0$ with $H_c = \tilde{H}_c$. This kind of coupling leads generally to two Dirac points in the combined surface dispersion relation, as plotted in Fig. 4. One Dirac point is just shifted by the coupling to the Weyl surface state. The other one is created out of the Weyl and Dirac states along a momentum direction where there is no coupling between these two bands. Under the assumption that both spin species couple equally strong to the WSM, $|\tilde{H}_c| = |H_c|$, there is always such a momentum direction ϕ_k where one part (hole or electron) of the Dirac cone is not coupled to the WSM surface state, while the other part is maximally coupled, see Eq. (3.9) above. For the lower, hole-like cone, using the parameters in Fig. 4, this direction is $\phi_k = -\frac{\pi}{2}$, thus the negative k_y axis with $k_x = 0$. The dispersion relation is then $E = C + Ak_y$ corresponding to the cyan line in Fig. 4 (a) which crosses the other two straight lines.

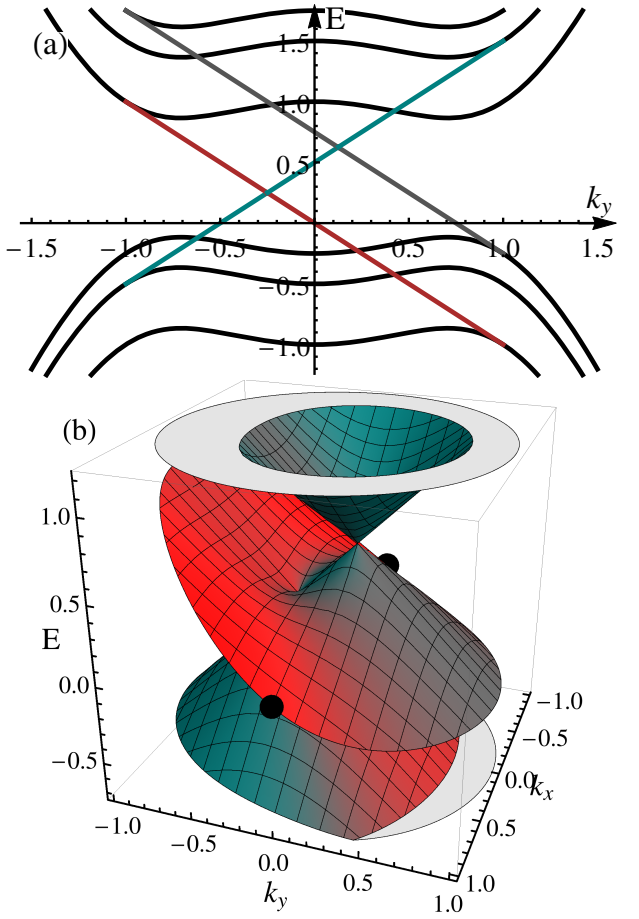

FIG. 4: (a) Bulk and upper surface dispersions relation of the TI & WSM model with real, spin-symmetric coupling. Color code: Black lines for the bulk states, red for WSM character and cyan for the TI character of the surface states. (b) 3D plot of the surface dispersion relation. Two Dirac points are visible.
Parameters: $C = \frac{1}{2}$, $M_0 = -1$, $M_1 = 1$, $B = 1$, $k_z = 0$, $\gamma = -\frac{1}{4}$, $A = 1$, $v_y = 1$, $a(k_\parallel) = \frac{1}{4}$, $b_1 = 0$, $H_c = \tilde{H}_c$.

Considering finite couplings $a_0 \neq 0$ or $b_1 \neq 0$ gives only quantitative differences in the dispersion relations (not shown). The Dirac point generation is unaffected,

except for the special case where the Dirac point and Fermi arc cross only at $k_x = k_y = 0$. As in this case the coupling for $b_1 \neq 0$ is absent in this point, no second Dirac point is generated.

A perturbative calculation can provide some insight into both kinds of Dirac points. We take the surface Hamiltonian, Eq. (3.8), and treat one band as a perturbation to the other two.

For the shifted Dirac point one directly finds in 2nd order perturbation theory in the coupling

$$H_D^1 = \begin{pmatrix} C & i\eta A k_- \\ -i\eta A^* k_+ & C \end{pmatrix} + \frac{1}{C - \gamma\left(M_0 + M_1 k_x^2\right) - \eta v_y k_y} \begin{pmatrix} |H_c|^2 & H_c \tilde{H}_c^* \\ \tilde{H}_c H_c^* & |\tilde{H}_c|^2 \end{pmatrix}. \tag{4.1}$$

Evidently, a difference in the absolute values of the coupling between the Weyl system and the different spin species of the TI system will open a gap. In the limit of spin degeneracy, where $H_c = \tilde{H}_c$, we insert the coupling from Eq. (3.4), expand Eq. (4.1) for small momenta and find

$$H_D^1 = \begin{pmatrix} C & i\eta A k_- \\ -i\eta A^* k_+ & C \end{pmatrix} + \frac{|a_0|^2}{C - \gamma M_0} \begin{pmatrix} 1 & 1 \\ 1 & 1 \end{pmatrix} + \mathcal{O}\left(k_\pm\right) \tag{4.2}$$

corresponding to a Dirac cone shifted in energy and momentum by the coupling. For real A the shift occurs in the k_y direction as shown in Fig. 4.

The creation of the second Dirac point can be understood from a similar calculation. The perturbative Hamiltonian for this Dirac point is given by

$$H_D^2 = \begin{pmatrix} C - |A|\, k_\parallel & \frac{1}{\sqrt{2}} H_c \left(1 - e^{i\phi_k^A}\right) \\ \frac{1}{\sqrt{2}} H_c^* \left(1 - e^{-i\phi_k^A}\right) & \gamma\left(M_0 + M_1 k_x^2\right) + \eta v_y k_y - |H_c|^2 \frac{1+\cos\left(\phi_k^A\right)}{C + |A| k_\parallel - \gamma(M_0 + M_1 k_x^2) - \eta v_y k_y} \end{pmatrix}. \tag{4.3}$$

The off-diagonal elements vanish along the momentum direction $\phi_k = \phi_A + \eta\frac{\pi}{2}$. Thus, Weyl and Dirac surface states are uncoupled in one point. This point becomes the new Dirac point, and setting the diagonal elements of Eq. (4.3) equal, this gives its precise value k_D. For the parameters used in Fig. 4, the Dirac point k_D is on the negative k_y axis, with the corresponding Hamiltonian

$$H_D^2 = \begin{pmatrix} C + A\left(k_D + k_y\right) & \frac{1}{\sqrt{2}} k_x \left(b_1 + i\frac{a_0}{k_D}\right) \\ \frac{1}{\sqrt{2}} k_x \left(b_1 - i\frac{a_0}{k_D}\right) & C + A\left(k_D - k_y\right) + 2 f_{di}(k_x, k_y) \end{pmatrix} \tag{4.4}$$

including the distortion $f_{di}(k_x, k_y) = (A - v_y)\, k_y + \frac{2b_1(a_0 k_x - x_1 k_D k_y) + A k_D k_y (A - v_y)}{C - (A - v_y) k_D - \gamma M_0}$ and $k_D = \frac{v_y(C - \gamma M_0) - \sqrt{2a_0^2\left(A^2 - v_y^2 - 2b_1^2\right) + \left(A^2 - 2b_1^2\right)(C - \gamma M_0)^2}}{A^2 - v_y^2 - 2b_1^2}$. The Dirac point is stable for any real combination of spin-symmetric couplings. A finite distortion $f_{di} \neq 0$ tilts the Dirac cone but does not open a gap.

The number of Dirac points in the surface dispersion relation can be extended further by a coupling that changes sign as a function of k_x and k_y, e.g. by setting $a_0 > 0$ and $a_2 < 0$ or a combination of $a_0 \neq 0$ and $b_1 \neq 0$. The positions in k-space where the coupling is zero and TI and WSM surface state intersect will then harbor additional Dirac points, see Fig. 5.

C. Spin-asymmetric coupling: Creation of gaps & spin polarization

The spin-up and spin-down TI bands do not need to have the same coupling to the WSM. If the absolute values are different, $|H_c| \neq |\tilde{H}_c|$, the Dirac points in the surface dispersion relation are gapped out, see Eq. (4.1) and Fig. 6. The bulk Weyl points are, however, unaffected. The resulting bands are partly spin polarized as shown in Fig. 6. The weaker coupled spin up electrons form a band with the Weyl surface state at intermediate energies, while the stronger coupled spin down electrons are pushed into the upper and lower bands. Considering a finite $b_1 \neq 0$ instead of a a_0 coupling, only the lower Dirac point will split. As the upper one is located at $k_x = k_y = 0$ for a pure momentum dependent coupling, the effective coupling between the WSM and TI surface states is zero here.

D. Phase-shifted coupling: Moving Dirac points, tilting dispersion relation

Including complex coupling constants, this offers additional ways to alter the bulk and surface spectrum. In general, the dispersion relation will look much less symmetric compared to the previous, real couplings.

Assuming $\tilde{H}_c = H_c$, one can directly conclude from the Hamiltonian in Eq. (3.9) that a complex coupling $A = i$ will lead to two Dirac points lying on the k_x, rather than

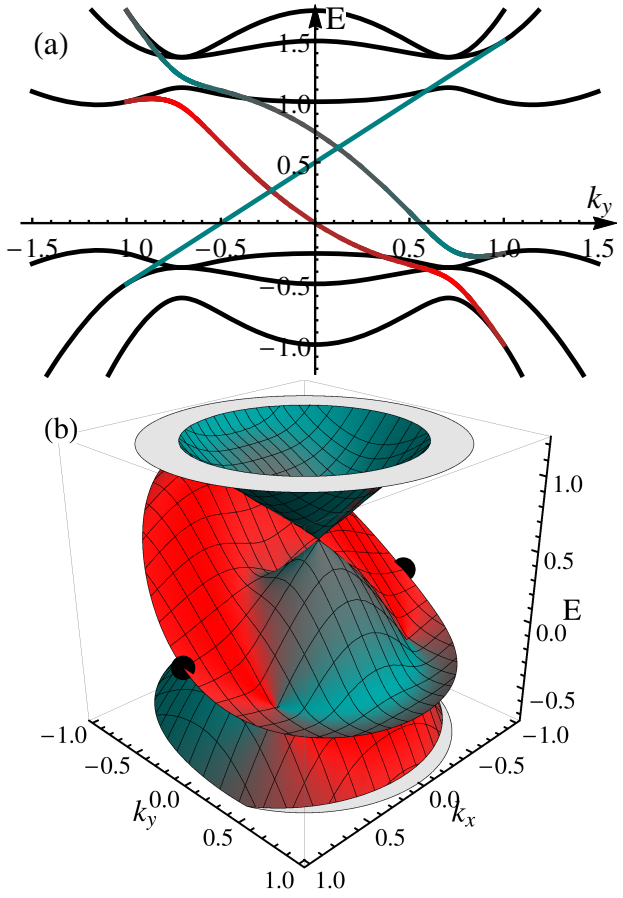

FIG. 5: (a) Bulk and upper surface dispersion relations of the TI and WSM models with a coupling that changes sign. Color code: Black lines for the bulk states, red for WSM character and cyan for the TI character of the surface states. (b) 3D plot of the surface dispersion relation. Four Dirac points are visible.
Parameters: $C = \frac{1}{2}$, $M_0 = -1$, $M_1 = 1$, $B = 1$, $k_z = 0$, $\gamma = -\frac{1}{4}$, $A = 1$, $v_y = 1$, $a_0 = \frac{1}{4}$, $a_2 = -\frac{1}{2}$, $b_1 = 0$, $H_c = \tilde{H}_c$.

on the k_y axis as discussed in Sec. IV B. This is confirmed in Fig. 7. One also sees that the bulk Weyl points lie not on the k_x axis, but are rotated by the complex coupling. Yet the rotation is much smaller than the $\pi/2$ rotation of the surface Dirac points.

The same effect is obtained by a complex phase difference between the couplings H_c and $\tilde{H}_c$. It can even undo the rotation induced by $A = i$. Note also that in the spin-symmetric case, already for real and finite $a(k_\parallel)$ and b_1 the Weyl points are rotated away from the k_x axis. Here the effective coupling is complex, with a phase changing with $k_\pm$. Supplementing this with a complex $a(k_\parallel)$, this can again lead to points where the effective coupling is zero, resulting in additional Dirac points like in Sec. IV B.

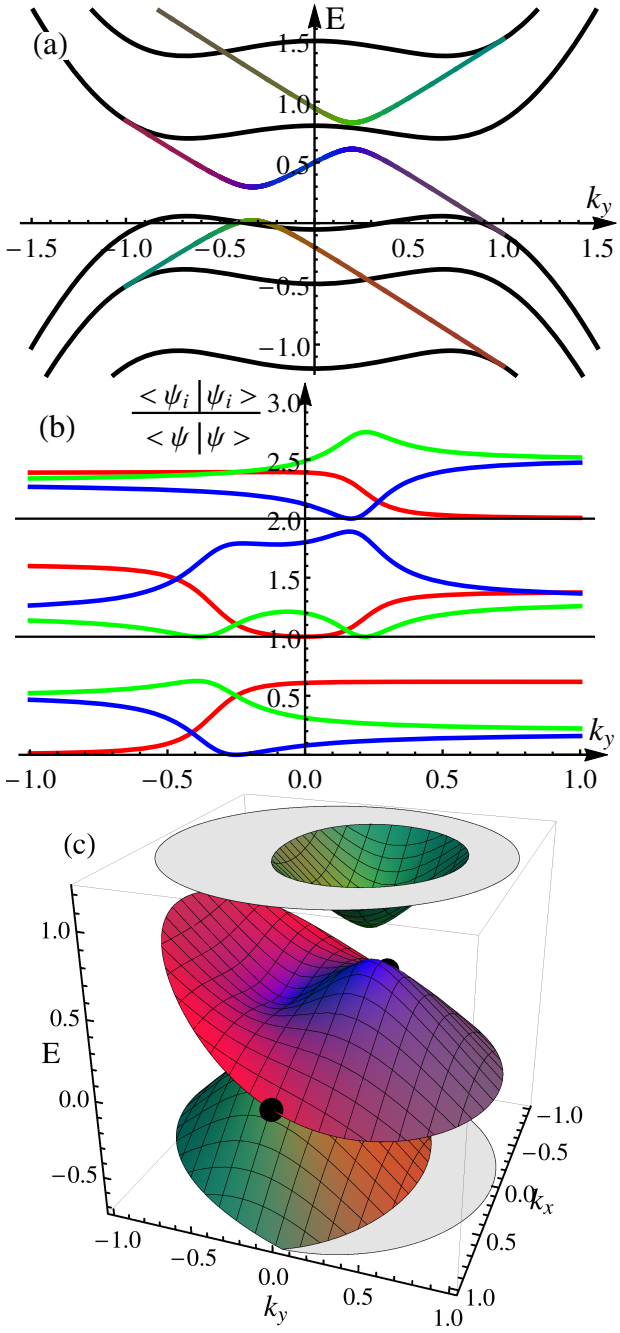

FIG. 6: (a) Bulk and upper surface dispersion relations of the TI and WSM model with an spin-asymmetric coupling. Color code: Black lines for the bulk states, red for WSM character and blue (green) for the TI spin up (down) character of the surface states. (b) Character of the three surface bands, shifted for clarity. (c) 3D plot of the surface dispersion relation. All Dirac points are gapped.
Parameters: $C = \frac{1}{2}$, $M_0 = -1$, $M_1 = 1$, $B = 1$, $k_z = 0$, $\gamma = -\frac{1}{4}$, $A = 1$, $v_y = 1$, $a(k_\parallel) = \frac{1}{4}$, $\tilde{a}(k_\parallel) = \frac{2}{4}$, $b_1 = \tilde{b}_1 = 0$.

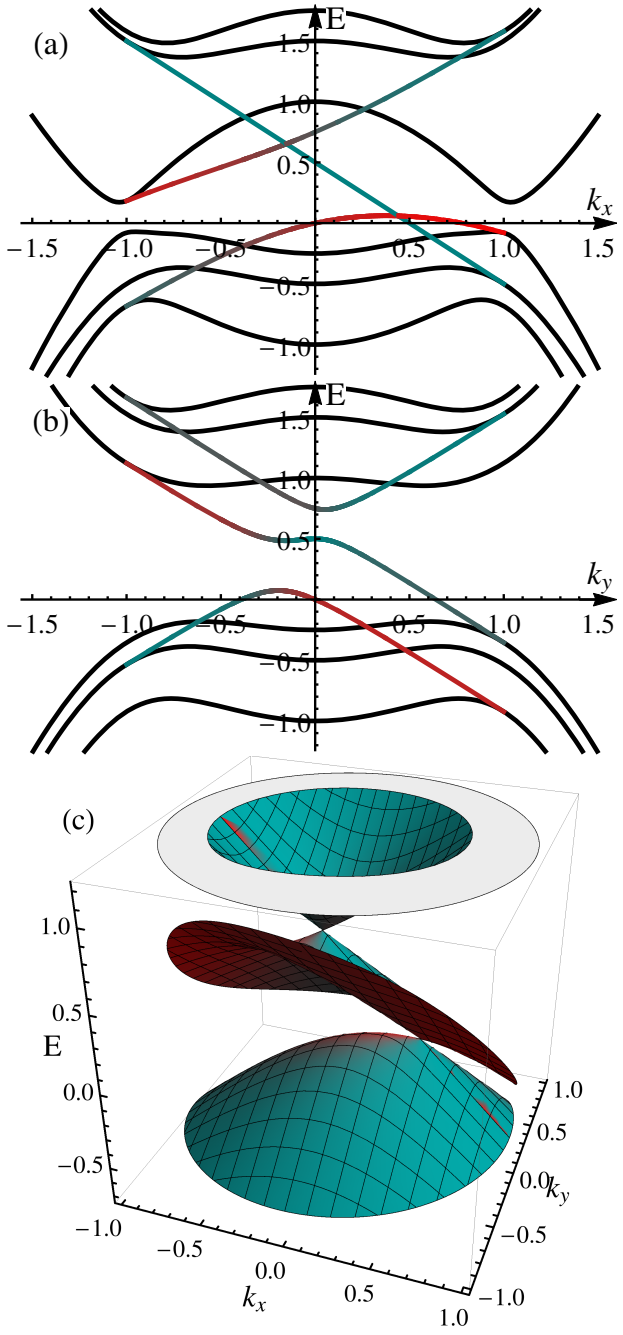

FIG. 7: (a) and (b) Bulk and upper surface dispersion relations of the TI and WSM model with a complex coupling. Color code: Black lines for the bulk states, red for WSM character and cyan for the TI character of the surface states. (c) 3D plot of the surface dispersion relation. Two Dirac points on the k_x axis are visible.
Parameters: $C = \frac{1}{2}$, $M_0 = -1$, $M_1 = 1$, $B = 1$, $k_z = 0$, $\gamma = -\frac{1}{4}$, $A = i$, $v_y = 1$, $a(k_\parallel) = \frac{1}{4}$, $b_1 = 0$, $H_c = \tilde{H}_c$.

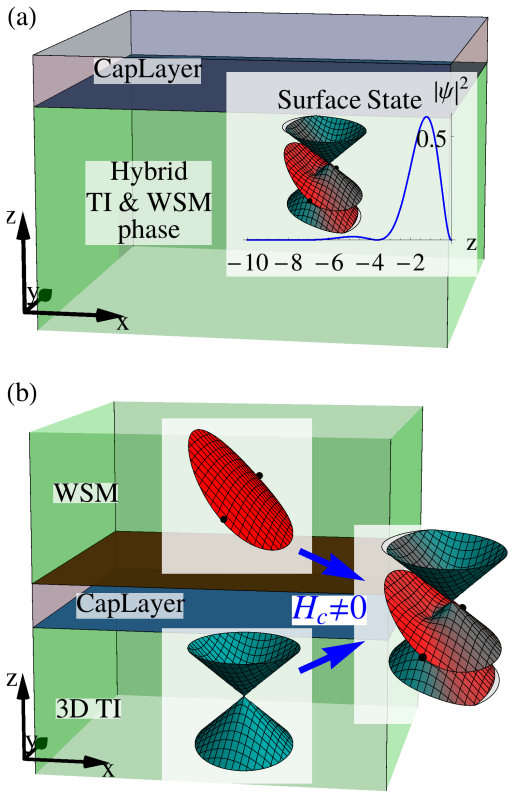

FIG. 8: Possible experimental realizations: (a) Bulk materials being in the combined 3D TI and WSM phase will naturally have hybrid surface states. (b) A heterostructure where TI and WSM phases are adjacent to each other will exhibit hybrid surface states for finite coupling $H_C \neq 0$, provided e.g. by Coulomb interaction or tunneling.

V. EXPERIMENTAL REALIZATION

We propose two ways to realize the physics of hybrid TI and WSM phases in an experimental setup. First, a material that naturally is in this combined phase will have corresponding surface states, as depicted in Fig. 8 (a). Compressively strained HgTe is a candidate material for this phase: the compressive strain pushes the Γ_8 bands against each other creating Weyl points[26], in addition to the prevailing topological band inversion between the Γ_8 and Γ_6 bands. A difference to our calculation is the preserved time-reversal symmetry, leading to eight Weyl points in HgTe instead of two. However, if HgTe is doped with Mn the number of Weyl points could be reduced by a (partial) magnetic ordering.

The second realization consists of a WSM in contact with a 3D TI, possibly separated by a thin buffer layer as depicted in Fig. 8 (b). This should lead to a hybrid surface state at the joint boundary. The finite coupling H_C could be provided by tunneling or Coulomb interaction. While this surface state is not exactly of the form of the ansatz in Eq. (3.5), the surface Hamiltonian, Eq. (3.8), should still be valid with the modification $\eta = \eta_{TI} = -\eta_W$. As several proposals of TRS-broken WSM with two Weyl points are based on magnetically doped 3D TI materials[33–36], the fabrication of the described hybrid system should be technically feasible.

VI. CONCLUSION & OUTLOOK

We have analyzed a hybrid system composed of a 3D TI coupled to an inversion symmetric, TRS-broken WSM. In the spirit of a tunnel coupling approach between the two topological phases, the use of a simplified ansatz made it possible to find an analytical solution for the surface states. The resulting surface Hamiltonian, Eq. (3.8), is a major result of this paper. The dispersion relation of the hybrid system shows different phenomena depending on the assumed coupling between WSM and TI. Preserved spin symmetry e.g. leads to the creation of additional Dirac points in the surface dispersion relation. Breaking of spin symmetry on the other hand, this opens gaps and induces spin polarization in the former Dirac surface cone. As an experimental realization we have presented both strained HgTe, which might naturally be in the discussed hybrid phase, and a heterostructure of TI and WSM. In the latter case, the joint boundary would harbor the interesting hybrid surface state.

There are several directions how to proceed with this research. Looking for measurable consequences, e.g. in transport or spectroscopy, of the new hybrid surface states should be the most immediate one. We expect, for instance, that different Dirac points will give rise to different minima in the conductivity, similar to the graphene case[52,53]. An extension to time-reversal symmetric WSM is another one. For this, one should use a 4x4 Hamiltonian for the WSM, which offers the possibility of more involved Fermi arcs on the surface, e.g. including spin polarization along the arcs[54,55]. $TaIrTe_4$[30,31] with its four Weyl points could be a candidate material for a hybrid system of this kind.

Acknowledgments

We thank C. Brüne, E. M. Hankiewicz, J. B. Mayer and M. Kharitonov for interesting discussions. We acknowledge financial support by the DFG (SPP 1666 and SFB 1170 "ToCoTronics"), the Helmholtz Foundation (VITI) as well as the ENB Graduate school on "Topological Insulators".

Appendix A: Hardwall boundary condition 2x2

In this section, we recap a simple method for calculating exponentially localized boundary states of a 2x2 Hamiltonian following Ref. 41 and references therein. We introduce hardwall boundary conditions on a half space $z \leq 0$ or $z \geq 0$. Thus, the surface state is localized at $z = 0$ and decays either in direction $z \to -\infty$ (upper surface) or $z \to +\infty$ (lower surface). The state should fulfill the eigenvalue equation

$$H\Psi(z) = E\Psi(z) \tag{A1}$$

with $H = \left[h_4\left(k_\parallel^2 + k_z^2\right) + h_3\right]\tau_3 + h_2 k_z \tau_2 + h_1(k_\pm)\tau_1 + h_0\tau_0$ and h_j being real constants or functions of $k_\pm$. The Hamiltonian can represent a topological insulator or Weyl semimetal depending on the chosen h_j.

The general ansatz for the eigenstate is

$$\Psi_g(z) = \sum_{j\in\{1,2\}} a_j e^{ik_{z,j}z}\psi(k_\pm, k_{z,j}), \tag{A2}$$

which could be used to solve for the surface states of Eq. (A1) in the usual manner. Due to the specific structure of our Hamiltonian, we can choose a simplified version of the ansatz, given by

$$\Psi(z) = \left(e^{ik_{z,1}z} - e^{ik_{z,2}z}\right)\psi(k_\pm). \tag{A3}$$

The relative sign ensures that the wave function vanishes at $z = 0$. The ansatz offers the possibility to separate Eq. (A1) into two parts

$$\left[h_1(k_\pm)\tau_1 + h_0\tau_0\right]\Psi(z) = E\tau_0\Psi(z) \tag{A4}$$

$$\{[h_4(k_\parallel^2 + k_z^2) + h_3]\tau_3 + h_2 k_z \tau_2\}\Psi(z) = 0. \tag{A5}$$

Eq. (A4) is independent of k_z and can be solved for the surface dispersion relation E, while the solution of Eq. (A5) defines the two quantized values of k_z needed for the surface eigenstate.

Following this procedure, $\psi(k_\pm) = f(k_\pm)\psi_\pm$ is taken to be proportional to the eigenstate of the τ_1 Pauli matrix, $\tau_1\psi_\pm = \pm\psi_\pm$ and

$$\psi_\pm = \frac{1}{\sqrt{2}}\begin{pmatrix} 1 \\ \pm 1 \end{pmatrix} \tag{A6}$$

with $f(k_\pm) = 1$. Using $\tau_2\psi_\pm = \mp i\psi_\mp$ and $\tau_3\psi_\pm = \psi_\mp$, Eq. (A5) reduces to the quadratic equation

$$h_4\left(k_\parallel^2 + k_z^2\right) + h_3 - \eta i h_2 k_z = 0 \tag{A7}$$

with $\eta = \pm$ the sign inherited from $\psi_\pm$. Solving for k_z, we find the two solutions

$$ik_{z,\frac{1}{2}} = \frac{1}{2h_4}\left[-\eta h_2 \pm \sqrt{4h_4\left(h_3 + h_4 k_\parallel^2\right) + h_2^2}\right]. \tag{A8}$$

In order to obtain a wave function, exponentially decaying of the form of Eq. (A3), both $ik_{z,\frac{1}{2}}$ need a real part of the same sign. For real h_j, this gives us the existence condition

$$h_4\left(h_3 + h_4 k_\parallel^2\right) < 0. \tag{A9}$$

Depending on the sign of h_2/h_4 and the direction in which the wave function should decay, $z \to +\infty$ or $z \to -\infty$, one chooses the corresponding eigenstate $\psi_\pm$, fixing

$$\eta = -\mathrm{sgn}\left(\frac{h_2}{h_4}\right),\ \text{top};\ \eta = \mathrm{sgn}\left(\frac{h_2}{h_4}\right),\ \text{bottom}. \tag{A10}$$

The surface dispersion relations and wave functions are then given by

$$E^{sur} = h_0 + \eta h_1 (k_\pm); \ \Psi(z) = \left(e^{ik_{z,1}z} - e^{ik_{z,2}z}\right)\psi_\eta. \tag{A11}$$

The localization length is $l_c = \max\left\{\left|1/\Re\left(ik_{z,\frac{1}{2}}\right)\right|\right\}$.

The surface solution described in this section fulfills the eigenvalue Eq. (A1) and is thus a valid, non-perturbative eigenstate of the Hamiltonian. Calculating the surface state with the general ansatz (A2), this gives the same dispersion relation as for the simplified ansatz (A3) for the TI model in Sec. II A.

Appendix B: Numerical validation of approximate solution method

In this article we use an analytical method to calculate the localized boundary states, described in App. A. It requires certain restrictions on the parameters of the coupled TI-Weyl Hamiltonian, such as the same localization length for both TI and Weyl phase and half of the symmetry allowed couplings to be zero, see Sec. III.

These constraints might seem quite restrictive. In order to proof the general applicability of our results, we have checked numerically that the neglected couplings have no qualitative effect on the surface band structure if kept reasonably small. The same is true for variations that alter the localization lengths of the subsystems. The numerical method is similar to the analytical approach: We solve for exponentially localized surface wave functions on the half space $z \leq 0$ or $z \geq 0$ with hard-wall boundary condition at $z = 0$. The differences to the approximate solution is the use of the full ansatz for the wave function, i.e.

$$\Psi_g(z) = \sum_{j\in\{1,\dots,6\}} a_j e^{ik_{z,j}z}\psi(k_\pm, k_{z,j}). \tag{B1}$$

As an example, we take the case of the generation of the second Dirac point, discussed in Sec. IV B and depicted in Fig. 4. Besides the finite $a_0 = \frac{1}{4}$, we add an additional coupling $d_0 = \frac{1}{8}$ or change the localization length of the Weyl Hamiltonian by setting $v_z = \frac{3}{4} \neq B = 1$ and $t = \frac{5}{4} \neq M_1 = 1$. The latter choice leads then to differing localization lengths of the separate systems of

$$ik_{z,TI} = \frac{1}{2}\left[\frac{B}{M_1} \pm \sqrt{4\left(k_\parallel^2 - 1\right) + \left(\frac{B}{M_1}\right)^2}\right], \tag{B2}$$

$$ik_{z,WSM} = \frac{1}{2}\left[\frac{v_z}{t} \pm \sqrt{4\left(k_\parallel^2 - 1\right) + \left(\frac{v_z}{t}\right)^2}\right]. \tag{B3}$$

The resultant dispersion relations are shown in Fig. 9, depicted by blue dots. The analytical solution for the $a_0 = \frac{1}{4}$ coupling alone is displayed as a continuous surface.

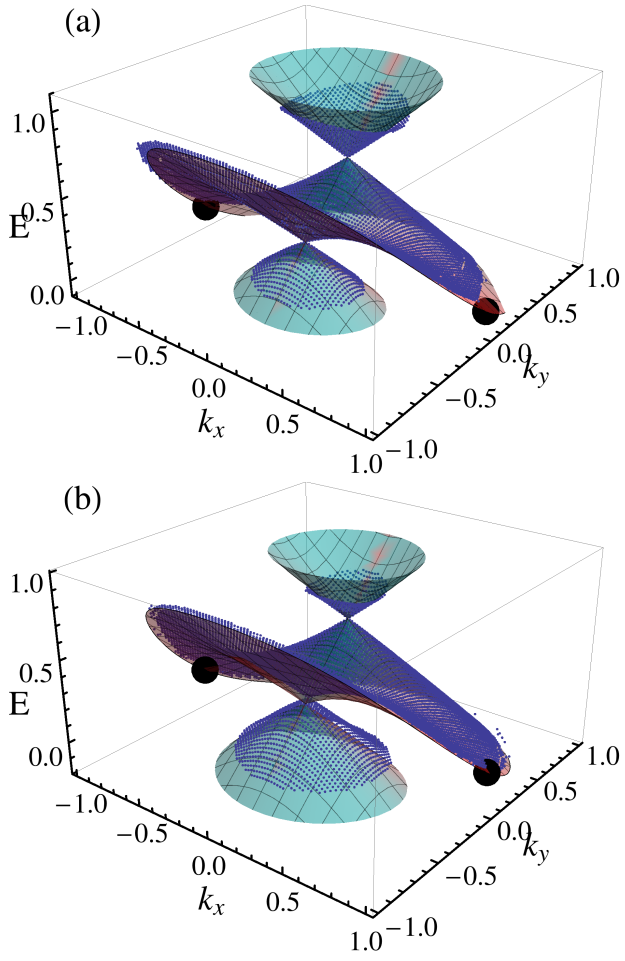

FIG. 9: Dispersion of the upper surface of the combined TI and WSM models. The continuous surface is the analytical solution from Fig. 4, the blue dots represent the full numerical solution. In (a) the additional coupling $d_0 = \frac{1}{8}$ was considered in the numerical solution, in (b) the altered parameters $v_z = \frac{3}{4} \neq B = 1$ and $t = \frac{5}{4} \neq M_1 = 1$. The large black dots denote the position of the Weyl notes of the analytical solution.

First we notice that the numerical and analytical solution agree very well and show no qualitative difference. The added coupling $d_0 = \frac{1}{8}$ in Fig. 9 (a) has almost no effect, the same was found for a finite $c_1 = \frac{1}{8}$. The changed localization length in Fig. 9 (b) shifts a bit the lower Dirac point, but does not open a gap. The major difference between the analytical and numerical solutions is the restriction of the surface solution to energies and momenta where no bulk state exists. This becomes especially clear for the upper and lower parts of the Dirac cone in Fig. 9, and is due to hybridization between the bulk and surface states. It prevents the existence of purely exponentially localized surface wave functions in this parameter range.

We conclude that the physical results and conclusions of this paper are valid beyond the restrictions on allowed couplings and localization lengths which are necessary to

keep the analytical form of the equations simple.

[1] M. Z. Hasan and C. L. Kane, Rev. Mod. Phys. **82**, 3045 (2010).
[2] X.-L. Qi and S.-C. Zhang, Rev. Mod. Phys. **83**, 1057 (2011).
[3] Y. Ando, J. Phys. Soc. Jpn. **82**, 102001 (2013).
[4] P. Hosur and X. Qi, C. R. Phys. **14**, 857-870 (2013).
[5] A. M. Turner and A. Vishwanath, Contemporary Concepts of Condensed Matter Science **6**, 293-324 (2013).
[6] S. Jia, S.-Y. Xu and M. Z. Hasan, Nat. Mat. **15**, 1140 (2016).
[7] B. Yan and C. Felser, Annu. Rev. Condens. Matter Phys. **8**, 1-19 (2017).
[8] H. B. Nielsen and M. Ninomiya, Phys. Lett. B **105**, 219 (1981).
[9] H. B. Nielsen and M. Ninomiya, Phys. Lett. B **130**, 389 (1983).
[10] S. Murakami, New Journal of Physics **9**, 356 (2007).
[11] X. Wan, A. M. Turner, A. Vishwanath and S. Y. Savrasov, Phys. Rev. B **83**, 205101 (2011).
[12] H. Weng, C. Fang, Z. Fang, B. A. Bernevig and X. Dai, Phys. Rev. X **5**, 011029 (2015).
[13] S.-M. Huang, S.-Y. Xu, I. Belopolski, C.-C. Lee, G. Chang, B. Wang, N. Alidoust, G. Bian, M. Neupane, C. Zhang, S. Jia, A. Bansil, H. Lin and M. Z. Hasan, Nat. Commun. **6**, 7373 (2015).
[14] S.-Y. Xu, N. Alidoust, I. Belopolski, Z. Yuan, G. Bian, T.-R. Chang, H. Zheng, V. N. Strocov, D. S. Sanchez, G. Chang, C. Zhang, D. Mou, Y. Wu, L. Huang, C.-C. Lee, S.-M. Huang, B. Wang, A. Bansil, H.-T. Jeng, T. Neupert, A. Kaminski, H. Lin, S. Jia and M. Z. Hasan, Nat. Phys. **11**, 748 (2015).
[15] L. Lu, Z.Wang, D. Ye, L. Ran, L. Fu, J. D. Joannopoulos and M. Soljačić, Science **349**, 622 (2015).
[16] S.-Y. Xu, I. Belopolski, N. Alidoust, M. Neupane, G. Bian, C. Zhang, R. Sankar, G. Chang, Z. Yuan, C.-C. Lee, S.-M. Huang, H. Zheng, J. Ma, D. S. Sanchez, B. Wang, A. Bansil, F. Chou, P. P. Shibayev, H. Lin, S. Jia and M. Z. Hasan, Science **349**, 613 (2015).
[17] B. Q. Lv, H. M. Weng, B. B. Fu, X. P. Wang, H. Miao, J. Ma, P. Richard, X. C. Huang, L. X. Zhao, G. F. Chen, Z. Fang, X. Dai, T. Qian and H. Ding, Phys. Rev. X **5**, 031013 (2015).
[18] B. Q. Lv, N. Xu, H. M. Weng, J. Z. Ma, P. Richard, X. C. Huang, L. X. Zhao, G. F. Chen, C. E. Matt, F. Bisti, V. N. Strocov, J. Mesot, Z. Fang, X. Dai, T. Qian, M. Shi and H. Ding, Nat. Phys. **11**, 724 (2015).
[19] L. X. Yang, Z. K. Liu, Y. Sun, H. Peng, H. F. Yang, T. Zhang, B. Zhou, Y. Zhang, Y. F. Guo, M. Rahn, D. Prabhakaran, Z. Hussain, S.-K. Mo, C. Felser, B. Yan and Y. L. Chen, Nat. Phys. **11**, 728 (2015).
[20] L. Huang, T. M. McCormick, M. Ochi, Z. Zhao, M.-T. Suzuki, R. Arita, Y. Wu, D. Mou, H. Cao, J. Yan, N. Trivedi and A. Kaminski, Nat. Mat. **15**, 1155 (2016).
[21] K. Deng, G. Wan, P. Deng, K. Zhang, S. Ding, E. Wang, M. Yan, H. Huang, H. Zhang, Z. Xu, J. Denlinger, A. Fedorov, H. Yang, W. Duan, H. Yao, Y. Wu, S. Fan, H. Zhang, X. Chen and S. Zhou, Nat. Phys. **12**, 1105 (2016).
[22] A. Tamai, Q. S. Wu, I. Cucchi, F. Y. Bruno, S. Riccò, T. K. Kim, M. Hoesch, C. Barreteau, E. Giannini, C. Besnard, A. A. Soluyanov and F. Baumberger, Phys. Rev. X **6**, 031021 (2016).
[23] J. Jiang, Z. K. Liu, Y. Sun, H. F. Yang, R. Rajamathi, Y. P. Qi, L. X. Yang, C. Chen, H. Peng, C.-C. Hwang, S. Z. Sun, S.-K. Mo, I. Vobornik, J. Fujii, S. S. P. Parkin, C. Felser, B. H. Yan and Y. L. Chen, Nat. Commun. **8**, 13973 (2017).
[24] N. Xu, Z. J. Wang, A. P. Weber, A. Magrez, P. Bugnon, H. Berger, C. E. Matt, J. Z. Ma, B. B. Fu, B. Q. Lv, N. C. Plumb, M. Radovic, E. Pomjakushina, K. Conder, T. Qian, J. H. Dil, J. Mesot, H. Ding and M. Shi, arXiv:1604.02116 (2016).
[25] Y. Sun, S.-C. Wu, M. N. Ali, C. Felser and B. Yan, Phys. Rev. B **92**, 161107(R) (2015).
[26] J. Ruan, S.-K. Jian, H. Yao, H. Zhang, S.-C. Zhang and D. Xing, Nat. Comm. **7**, 11136 (2016).
[27] J. Ruan, S.-K. Jian, D. Zhang, H. Yao, H. Zhang, S.-C. Zhang and D. Xing, Phys. Rev. Lett. **116**, 226801 (2016).
[28] G. Chang, S.-Y. Xu, D. S. Sanchez, S.-M. Huang, C.-C. Lee, T.-R. Chang, H. Zheng, G. Bian, I. Belopolski, N. Alidoust, H.-T. Jeng, A. Bansil, H. Lin and M. Z. Hasan, Sci. Adv. 2, e1600295 (2016).
[29] T. Rauch, S. Achilles, J. Henk and I. Mertig, Phys. Rev. Lett. **114**, 236805 (2015).
[30] I. Belopolski, P. Yu, D. S. Sanchez, Y. Ishida, T.-R. Chang, S. S. Zhang, S.-Y. Xu, D. Mou, H. Zheng, G. Chang, G. Bian, H.-T. Jeng, T. Kondo, A. Kaminski, H. Lin, Z. Liu, S. Shin and M. Z. Hasan, arXiv:1610.02013 (2016).
[31] K. Koepernik, D. Kasinathan, D. V. Efremov, S. Khim, S. Borisenko, B. Büchner and J. van den Brink, Phys. Rev. B **93**, 201101(R) (2016).
[32] S. Borisenko, D. Evtushinsky, Q. Gibson, A. Yaresko, T. Kim, M. N. Ali, B. Büchner, M. Hoesch and R. J. Cava, arXiv:1507.04847 (2015).
[33] A. A. Burkov and L. Balents, Phys. Rev. Lett. **107**, 127205 (2011).
[34] G. Y. Cho, arXiv:1110.1939 (2011).
[35] G. Xu, H. Weng, Z. Wang, X. Dai and Z. Fang, Phys. Rev. Lett. **107**, 186806 (2011).
[36] D. Bulmash, C.-X. Liu and X.-L. Qi, Phys. Rev. B **89**, 081106(R) (2014).
[37] Z. Wang, M.G. Vergniory, S. Kushwaha, M. Hirschberger, E. V. Chulkov, A. Ernst, N. P. Ong, R. J. Cava and B. A. Bernevig, Phys. Rev. Lett. **117**, 236401 (2016).
[38] R. Okugawa and S. Murakami, Phys. Rev. B **89**, 235315 (2014).
[39] A. G. Grushin, J. W. F. Venderbos and J. H. Bardarson, Phys. Rev. B **91**, 121109(R) (2015).
[40] H. Zhang, C.-X. Liu, X.-L. Qi, X. Dai, Z. Fang and S.-C. Zhang, Nat. Phys. **5**, 438 (2009).
[41] C.-X. Liu, X.-L. Qi, H. Zhang, X. Dai, Z. Fang and S.-C. Zhang, Phys. Rev. B **82**, 045122 (2010).
[42] K.-Y. Yang, Y.-M. Lu, and Y. Ran, Phys. Rev. B **84**, 075129 (2011).
[43] T. M. McCormick, I. Kimchi and N. Trivedi, arXiv:1604.03096 (2016).
[44] Y. Xu, F. Zhang and C. Zhang, Phys. Rev. Lett. **115**,

265304 (2015).
[45] A. A. Soluyanov, D. Gresch, Z. Wang, Q. Wu, M. Troyer, X. Dai and B. A. Bernevig, Nature **527**, 495 (2015).
[46] G. Sharma, P. Goswami and S. Tewari, arXiv:1608.06625 (2016).
[47] V. Dwivedi and S. T. Ramamurthy, Phys. Rev. B **94**, 245143 (2016).
[48] Y. Baum, T. Posske, I. C. Fulga, B. Trauzettel and A. Stern, Phys. Rev. Lett. **114**, 136801 (2015).
[49] E. Y. Ma, M. R. Calvo, J. Wang, B. Lian, M. Mühlbauer, C. Brüne, Y.-T. Cui, K. Lai, W. Kundhikanjana, Y. Yang, M. Baenninger, M. König, C. Ames, H. Buhmann, P. Leubner, L. W. Molenkamp, S.-C. Zhang, D. Goldhaber-Gordon, M. A. Kelly and Z.-X. Shen, Nat. Comm. **6**, 7252 (2015).
[50] M. Kharitonov, S. Juergens and B. Trauzettel, Phys. Rev. B **94**, 035146 (2016).
[51] P. Michetti, J. C. Budich, E. G. Novik and P. Recher, Phys. Rev. B **85**, 125309 (2012).
[52] M. I. Katsnelson, Eur. Phys. J. B **51**, 157 (2006).
[53] J. Tworzydło, B. Trauzettel, M. Titov, A. Rycerz, and C. W. J. Beenakker, Phys. Rev. Lett. **96**, 246802 (2006).
[54] B. Q. Lv, S. Muff, T. Qian, Z. D. Song, S. M. Nie, N. Xu, P. Richard, C. E. Matt, N. C. Plumb, L. X. Zhao, G. F. Chen, Z. Fang, X. Dai, J. H. Dil, J. Mesot, M. Shi, H. M. Weng and H. Ding, Phys. Rev. Lett. **115**, 217601 (2015).
[55] S.-Y. Xu, I. Belopolski, D. S. Sanchez, M. Neupane, G. Chang, K. Yaji, Z. Yuan, C. Zhang, K. Kuroda, G. Bian, C. Guo, H. Lu, T.-R. Chang, N. Alidoust, H. Zheng, C.-C. Lee, S.-M. Huang, C.-H. Hsu, H.-T. Jeng, A. Bansil, T. Neupert, F. Komori, T. Kondo, S. Shin, H. Lin, S. Jia and M. Z. Hasan, Phys. Rev. Lett. **116**, 096801 (2016).